CAV2021
11th International Symposium on Cavitation
May 10-13, 2021, Daejon, Korea

Optimal Control of Encapsulated Microbubbles for Biomedicine

Fathia F. Arifi[1] and Michael L. Calvisi[1*]

[1]Deparment of Mechanical and Aerospace Engineering, University of Colorado Colorado Springs, USA

Abstract: Encapsulated microbubbles (EMBs) were originally developed as contrast agents for ultrasound imaging but are more recently emerging as vehicles for intravenous drug and gene delivery. Ultrasound can excite nonspherical oscillations, or shape modes, that can enhance the acoustic signature of an EMB and also incite rupture, which promotes drug and gene delivery at targeted sites (e.g., tumors). Therefore, the ability to control shape modes can improve the efficacy of both the diagnosis and treatment mediated by EMBs. This work uses optimal control theory to determine the ultrasound input that causes EMB rupture with a minimum amount of acoustic input, in order to enhance patient safety and reduce unwanted side effects. The optimal control problem is applied to a model of an EMB that accounts for small amplitude shape deformations. This model is solved subject to a cost function that maximizes the incidence of rupture and minimizes the acoustic energy input. The optimal control problem is solved numerically through pseudospectral collocation methods using commercial optimization software. Single frequency and broadband acoustic forcing schemes are explored and compared. The results show that broadband forcing significantly reduces the acoustic effort required to incite EMB rupture relative to single frequency schemes. Furthermore, the acoustic effort required depends strongly on the shape mode that is forced to become unstable.

Keywords: ultrasound contrast agents, nonspherical bubbles, optimal control

1. Introduction

Encapsulated microbubbles (EMBs) are on the order of 1-10 μm in diameter and consist of a gas interior surrounded by a thin shell of lipid, polymer, or protein. Originally developed as ultrasound contrast agents (UCAs), EMBs are more recently being explored for therapeutic use as vehicles for drug and gene delivery, and tissue destruction (thrombolysis). EMBs can deform nonspherically under the direct action of ultrasound (US) or due to asymmetries in the blood flow caused by vessel walls or nearby bubbles. These nonspherical shape modes can enhance the acoustic echo of EMBs and improve image contrast. If sufficiently large, they can cause rupture of the EMB shell, which is undesirable for US imaging, but can help to release the EMB contents and promote drug and gene delivery. For safety reasons and to reduce unwanted side effects, the intensity of the driving acoustic pressure must be limited to avoid tissue damage due to US exposure [1,2]. One challenge facing scientists remains how to optimally control these transport vehicles. In clinical applications, single-frequency transducers with fixed amplitude are used; however, the use of more complex forcing schemes could provide benefits. The goal of this work is to apply optimal control theory to determine the minimal acoustic forcing required to incite rupture of EMBs. Various acoustic forcing schemes are applied to a model for small-amplitude shape perturbations of an EMB – including single frequency with both fixed and variable amplitude, and broadband acoustic forcing – and the total acoustic efforts are compared.

2. Methods

* Corresponding Author: Michael L. Calvisi, mcalvisi@uccs.edu

2.1. Analytical Model for Nonspherical EMB Oscillations

We briefly describe a model by Liu et al. [3] of small nonspherical oscillations of a single encapsulated microbubble with initial radius, R_0, as shown in Figure 1. The EMB is suspended in a liquid with constant properties of density, ρ, and viscosity, μ_l. We use spherical coordinates (r, θ, ϕ) in which θ and ϕ represent the polar and azimuthal angles, respectively. We assume the system is axisymmetric, so that that it is independent of ϕ, i.e., $\partial/\partial\phi = 0$. The surface of the EMB can deform in both the radial and tangential directions, and its surface position (r_s, θ_s) is represented as a perturbed sphere of radius, $R(t)$, superposed with small perturbations in the radial and tangential directions. These perturbations are expanded in a series of Legendre polynomials, $P_k(\cos\theta)$, and associated Legendre polynomials, $P_k^1(\cos\theta) = dP_k(\cos\theta)/d\theta$, according to

$$r_s(\theta, t) = R(t) + \sum_{k=2}^{\infty} a_k(t) P_k(\cos\theta), \qquad \theta_s(\theta, t) = \theta + \frac{1}{R(t)} \sum_{k=1}^{\infty} b_k(t) P_k^1(\cos\theta) \tag{1}$$

where $a_k(t)$ and $b_k(t)$ represent the amplitudes of the radial and tangential surface perturbations, respectively, and k is the mode number. We assume small perturbations, such that $a_k(t) \ll R(t)$ and $b_k(t) \ll R(t)$. Note that we neglect the $k = 1$ mode for the radial perturbation because this represents bubble translation, which is neglected here.

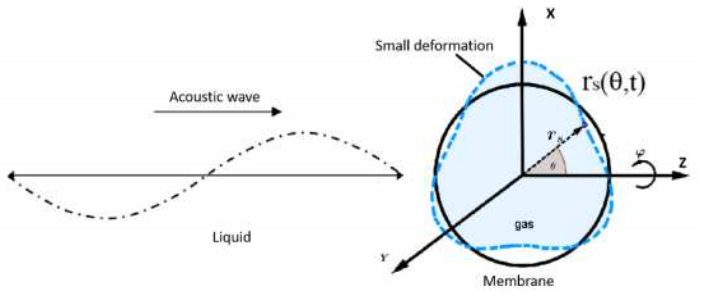

Figure 1. Schematic of an encapsulated microbubble (EMB) subject to forcing by an acoustic wave and undergoing small nonspherical deformations. The membrane surface position is denoted by the distance $r_s(\theta, t)$ from the origin.

The EMB oscillates in response to a time-varying far-field pressure, $p_\infty(t)$, of the following form:

$$p_\infty(t) = p_0\big(1 - F(t)\big) \tag{2}$$

where $F(t)$ represents the applied pulse excitation, and p_0 is the hydrostatic pressure. We refer to positive $F(t)$ as rarefactions and negative $F(t)$ as compressions. The radial dynamics, $R(t)$, of the EMB subject to acoustic driving $F(t)$ is governed by an equation similar to the Rayleigh–Plesset equation (RPE) but that includes additional terms to account for the membrane stress and viscous damping:

$$G_0 = R\ddot{R} + \frac{3}{2}\dot{R}^2 + \frac{1}{\rho}\left[\frac{2\gamma}{R} + \frac{4\mu_l\dot{R}}{R} - p_{g0}\left(\frac{R_0}{R}\right)^{3\Gamma} + p_\infty + 2G_s\frac{(R^6 - R_0^6)}{R^7} + \frac{4\mu_s\dot{R}}{R^2}\right] = 0 \tag{3}$$

where $\dot{R}$ and $\ddot{R}$ are the radial velocity and acceleration of the bubble wall, respectively, G_s is the shell elastic modulus, Γ is the effective polytropic index, which includes thermal dissipation, γ is surface tension, μ_s is the shell membrane viscosity, and p_{g0} is the initial gas pressure. Liu et al. derive evolution equations governing the radial and tangential deformations to first order in a_k and b_k, resulting in integrodifferential equations that involve integrals of the toroidal component of the vorticity. To simplify the governing equations and reduce the computational effort required to solve them, the integral terms are approximated. Since vorticity is generally considerable only within a small boundary layer around the bubble, the integral

* Corresponding Author: Michael L. Calvisi, mcalvisi@uccs.edu

terms can be approximated by multiplying the integrand value at the bubble wall times the boundary layer thickness [4]. Thus, we assume that the flow is irrotational in the bulk volume and that viscous effects are restricted to a thin boundary layer near the EMB surface. The thickness of the boundary layer is defined as $\chi = \min\left(\sqrt{\mu_l/\rho\omega_0}, (R/2k)\right)$ [5]. Using this boundary layer approximation, the governing equations for the radial and tangential shape modes reduce to

$$G_k = \ddot{a}_k + C_{aa}\dot{a}_k + C_{bb}\dot{b}_k + C_a a_k + C_b b_k = 0 \tag{4}$$

$$H_k = D_{aa}\dot{a}_k + D_{bb}\dot{b}_k + D_a a_k + D_b b_k = 0 \tag{5}$$

where C_{aa}, C_{bb}, C_a, C_b, D_{aa}, D_{bb}, D_a, and D_b are time-varying coefficients that depend on $R(t)$ and its time derivatives, thereby indicating parametric driving by the radial mode; for details, see [3,6].

Dimensionless variables are formed using the initial radius, R_0, the hydrostatic pressure, p_0, and a time, T_s, which is chosen to equal the period of the natural frequency of the radial mode, ω_0. This yields a dimensionless time, τ, dimensionless radius, r, and dimensionless amplitudes of the normal and tangential deformations, α_k and β_k, respectively, defined as follows: $t = T_s\tau$, $R = R_0 r$, $a_k = R_0\alpha_k$, and $b_k = R_0\beta_k$.

2.2. Optimal Control Problem

We seek to induce bubble rupture with minimal acoustic effort applied, which is defined by

$$Effort = \int_0^{t_f} [F(t)]^2\, dt. \tag{6}$$

We define bubble rupture as occurring when the amplitude one of the radial shape modes equals or exceeds the instantaneous radius, i.e., when $|a_k|/R(t) \geq 1$ or, equivalently, $|\alpha_k|/r(t) \geq 1$. We consider only shape modes $k = 2$ to $k = 5$, as higher-order modes dampen out more quickly due to viscosity and are less likely to manifest. Therefore, the optimal control problem is to seek a time-dependent driving that minimizes the acoustic effort and incites rupture at the final time, while identically satisfying the evolution equations for the radius, and normal and tangential shape deformations, such that $G_0 = 0$, $G_k = 0$, and $H_k = 0$ for $k = 2$ to 5. The time duration of the forcing is an unknown that is solved along with the rest of the problem. To solve this optimal control problem numerically, we use the commercial software TOMLAB PROPT, which uses pseudospectral collocation methods. In order to get a solution, initial guesses must be provided for the acoustic forcing, $F(\tau)$, over the dimensionless time period and also for the solutions of $r(\tau)$, $\alpha(\tau)$, and $\beta(\tau)$. We explore three acoustic forcing schemes, which are listed below:

1. Fixed-amplitude single-frequency (FASF) forcing, $F(t) = \varepsilon \sin(\omega_d t)$, where ε is constant.
2. Variable-amplitude single-frequency (VASF) forcing, $F(t) = \varepsilon(t) \sin(\omega_d t)$, where $\varepsilon(t)$ is variable in time.
3. Broadband (unconstrained) forcing, $F(t)$.

For the two single-frequency forcing cases, we set $\omega_d = \omega_0$, which is the natural frequency of the radial mode, because this was determined to be the most effective frequency at causing shape instability.

3. Results

We optimize the response of an encapsulated microbubble with initial radius R_0 = 2 μm and the external fluid is assumed to be water with the following properties: ρ = 1000 kg/m^3, μ_l = 0.01 Pa-s, p_0 = 101,325 Pa, γ = 0.073 N/m, G_s = 0.1 N/m, and vapor pressure p_v = 2,337 Pa. Our main interest is in lipid-

* Corresponding Author: Michael L. Calvisi, mcalvisi@uccs.edu

coated EMBs, which are comprised of a monolayer with negligible thickness, therefore, we set the shell bending modulus $G_b = 0$. We assume the EMB is initially stationary with a small radial perturbation, such that $r(0) = 1$, $r'(0) = 0$, $\alpha_k(0) = 0.1$, and $\beta_k(0) = 0$ for $k = 2$ to 5, and that the forcing is initially zero, $F(0) = 0$. Due to limitations in the TOMLAB PROPT software, we investigate the optimal solution for the instability criteria, $|\alpha_k|/r \geq 1$, as separate cases for $k = 2$ to 5.

Plots of the dimensionless radius, $r(t)$, acoustic forcing, $F(t)$, and shape mode amplitudes vs. time are shown in Figures 2 and 3 for the cases of fixed-amplitude single-frequency (FASF) forcing and broadband (unconstrained) forcing, respectively. The instability criteria specified for these figures was $|\alpha_2|/r \geq 1$. Plots for other instability criteria are qualitatively similar and are not shown for the sake of brevity.

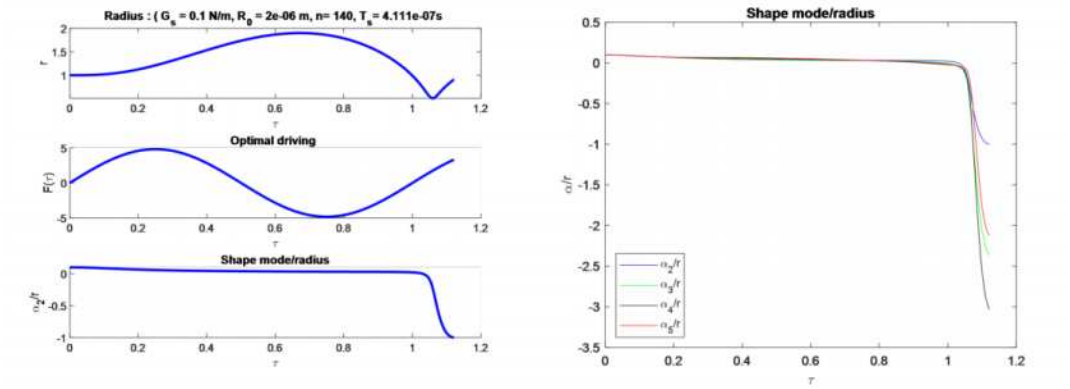

Figure 2. Left: Plots of the dimensionless radius, optimal driving, and second-order shape modes vs. dimensionless time from the solution of the optimal control problem for instability criteria $|\alpha_2|/r \geq 1$ by applying fixed-amplitude single-frequency forcing. Right: Plots of all shape modes vs. time.

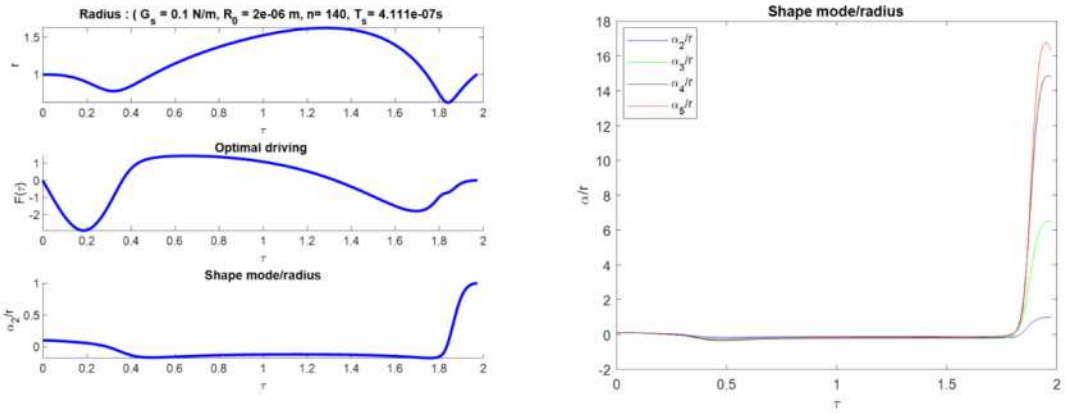

Figure 3. Left: Plots of the dimensionless radius, optimal driving, and second-order shape modes vs. dimensionless time from the solution of the optimal control problem for instability criteria $|\alpha_2|/r \geq 1$ by applying broadband forcing. Right: Plots of all shape modes vs. time.

The minimal dimensionless acoustic effort required to induce instability for each acoustic forcing scheme and each instability criteria is tabulated in Table 1. Two trends are evident from this data. First, for a fixed instability criteria, the minimum acoustic effort decreases as the forcing scheme is changed progressively from FASF to variable-amplitude single-frequency (VASF) forcing to broadband forcing. This suggests that the greater the degrees of freedom available in the acoustic forcing, the less the acoustic effort is required to cause EMB rupture. Second, for a given forcing scheme, the effort required reduces as

* Corresponding Author: Michael L. Calvisi, mcalvisi@uccs.edu

the shape mode number that is forced to become unstable is increased. In other words, less effort is required to force higher-order shape modes to become unstable. For example, the effort required to force α_5 to become unstable requires between 2-5 times less effort than forcing α_2 to become unstable.

Table 1. Minimum dimensionless acoustic effort required to incite rupture.

Instability Criteria	Fixed-Amplitude Single-Frequency Forcing	Variable-Amplitude Single-Frequency Forcing	Broadband Forcing
$\lvert\alpha_2\rvert/r \geq 1$	12.16	8.143	3.426
$\lvert\alpha_3\rvert/r \geq 1$	3.990	2.974	1.958
$\lvert\alpha_4\rvert/r \geq 1$	2.641	2.105	1.722
$\lvert\alpha_5\rvert/r \geq 1$	2.321	1.926	1.719

Acknowledgments: The authors acknowledge NSF CAREER Award 1653992 for providing funding support.

References

1. Phipps, N. Acoustic Intensity Measurement System: Application in Localized Drug Delivery. M.S., San Jose State University, San Jose, California, USA, 2010.
2. Reddy, A.J.; Szeri, A.J. Optimal pulse-inversion imaging for microsphere contrast agents. *Ultrasound in Medicine and Biology* **2002**, *28*, pp. 483–494.
3. Liu, Y.; Sugiyama, K.; Takagi, S.; Matsumoto, Y. Surface instability of an encapsulated bubble induced by an ultrasonic pressure wave. *Journal of Fluid Mechanics* **2012**, *691*, pp. 315–340.
4. Klapcsik, K.; Hegedus, F. Study of non-spherical bubble oscillations under acoustic irradiation in viscous liquid. *Ultrasonics Sonochemistry* **2019**, *54*, pp. 256– 273.
5. Hilgenfeldt, S.; Lohse, D.; Brenner, M.P. Phase diagrams for sonoluminescing bubbles. *Physics of Fluids* **1996**, *8*, pp. 2808-2826.
6. Arifi, F.F. Stability Analysis and Optimal Control of the Nonspherical Oscillation of Encapsulated Microbubbles for Biomedicine. Ph.D., University of Colorado Colorado Springs, Colorado Springs, Colorado, USA, 2020.

* Corresponding Author: Michael L. Calvisi, mcalvisi@uccs.edu